

Influence of colloidal fouling on rejection of trace organic contaminants by reverse osmosis

How Y. Ng^a, Menachem Elimelech^{b,*}

^a Centre for Water Research, Department of Civil Engineering, National University of Singapore, Block EIA #07-03, No. 1 Engineering Drive 2, S117576, Singapore

^b Department of Chemical Engineering, Environmental Engineering Program, Yale University, P.O. Box 208286, New Haven, CT 06520-8286, USA

Received 15 January 2004; received in revised form 16 June 2004; accepted 23 June 2004

Available online 11 September 2004

Abstract

A systematic investigation on the influence of colloidal fouling on removal of trace organics (steroid hormones) and inert organics by reverse osmosis (RO) membranes is reported. Results of laboratory-scale crossflow membrane filtration experiments showed that colloidal fouling caused a marked decrease in rejection of inert organic molecules with molecular weight smaller than about 100 g/mol. While the removal of inert organics was mainly due to steric (size) exclusion, adsorption and diffusion across the membrane polymer played a prominent role in the removal of the steroid hormones by the RO membrane. During membrane fouling, rejection of the inert organics and salt declined to a minimum, but then improved slowly and eventually stabilized at a fixed value. Hormone rejection, on the other hand, decreased rapidly initially, and then gradually slowed down regardless of fouling. This rejection behavior is associated with the decrease in feed hormone concentration due to adsorption and the increase in permeate concentration due to diffusion across the membrane skin layer. The decline in hormone rejection with time was much more severe when colloidal fouling took place. The solute rejection behavior is markedly influenced by the cake-enhanced concentration polarization, whereby the colloidal cake layer hinders back diffusion of solutes from the membrane surface to the bulk solution. The buildup of solutes at the membrane surface results in a higher solute concentration gradient across the membrane and, thus, a greater solute transport through the membrane and a lower observed solute rejection. The rate of decline in permeate flux and solute (hormones, inert organics, and salt) rejection correlated inversely with channel wall shear rate.

© 2004 Elsevier B.V. All rights reserved.

Keywords: Reverse osmosis; Colloidal fouling; Solute rejection; Flux decline; Trace organic contaminants; Hormones; Concentration polarization; Cake-enhanced concentration polarization

1. Introduction

Fouling is an inevitable phenomenon in reverse osmosis (RO) systems used in various water quality control applications. Membrane fouling results in several deleterious effects, including a decrease in water production because of a gradual decline in flux, an increase in applied pressure required for a constant rate of water production, a gradual membrane degradation which results in a shorter membrane life, and a decrease in permeate quality.

Numerous studies have been reported on colloidal fouling with emphasis on permeate flux decline [1–7]. Cohen and Probststein [3] investigated the fouling rate of cellulose acetate RO membranes by colloidal ferric hydroxide in deionized water. Their work demonstrated a linear relationship between permeate flux and foulant layer thickness during the initial stages of fouling. In a recent study, Hoek et al. [7] found that flux decline in colloidal fouling of RO and NF membranes is primarily due to “cake-enhanced osmotic pressure”. They suggested that a severe flux decline was observed because the colloidal cake layer limits back diffusion of salt ions from the membrane surface to the bulk solution, thus significantly elevating salt concentration

* Corresponding author. Tel.: +1 203 432 2789; fax: +1 203 432 2881.
E-mail address: menachem.elimelech@yale.edu (M. Elimelech).

at the membrane surface and the trans-membrane osmotic pressure.

To minimize fouling, pretreatment is frequently applied with the goal of eliminating foulants from the feed water. However, pretreated feed water may still contain dissolved organic compounds and small colloidal particles such as clay, silica, and organic matter which contribute to RO membrane fouling [8]. Sugahara et al. [1] and Winfield [2] have determined that larger particles do not contribute significantly to fouling and that fouling is controlled by small colloidal particles. Winfield [2] found that dissolved colloidal materials in secondary wastewater effluents, but not large suspended particles ($>5 \mu\text{m}$), contributed significantly to RO membrane fouling. Sugahara et al. [1] concluded that particles smaller than $0.45 \mu\text{m}$, including true colloids and dissolved solids, contribute the most to RO membrane fouling.

Membrane rejection of organic compounds has been extensively studied in recent years [9–15]. The rejection of organics depends on membrane properties such as pore size, membrane material, and membrane charge; solute characteristics such as molecular size, charge, and polarity; and feed solution chemistry. With the increase usage of secondary wastewater effluent as a source water for advanced water reuse by RO separation, the effectiveness of RO in rejecting trace organic compounds becomes rather important. Removal of trace organics in reclaimed water is a major concern since it is now recognized that trace organics – such as hormones which have the greatest endocrine disrupting potency among all endocrine disrupting chemicals – cause adverse health effects to humans and animals [16–22].

A number of studies have concluded that membrane fouling may either improve or deteriorate permeate water quality [23–26]. Lipp et al. [23] reported that fouling of RO membranes by iron hydroxide caused a decrease in salt rejection, whereas fouling by humic substances resulted in an improvement of salt rejection. In another study, van Oers et al. [24] showed that, in the presence of a relatively open silica deposit, a marked decrease in polyethylene glycol (PEG) and dextran rejections was observed compared to the rejection of a clean ultrafiltration membrane. However, an increase in PEG rejection occurred in the presence of a bovine serum albumin deposit. It was suggested that solute rejection is dependent on the relative solute selectivities of the fouling layer and the membrane. Two different cases were distinguished in that study. First, when the membrane rejects solutes better than the deposited layer, hindered back diffusion of solutes by the fouling layer would cause solute to accumulate near the membrane surface. This enhanced concentration polarization results in greater concentration gradient across the membrane and, hence, a decrease in solute rejection. Second, when solutes are rejected better by the deposited layer than the membrane, the fouling layer controls solute rejection and solute rejection improves.

For colloidal fouling of RO or NF membranes, the first case discussed above is most likely the predominant fouling mechanism governing membrane performance. This explains

the increase in salt passage through the fouled membrane reported by Jackson and Landolt [25], and Staude and Assenmacher [26]. A decrease in solute rejection due to membrane fouling, even by a few percent, can compromise the quality and safety of water for further application. Despite the importance of this problem, it is surprising that no studies are available on the effect of colloidal fouling on trace organic removal by RO or NF membranes. Therefore, systematic studies on the influence of fouling on the rejection behavior of low molecular weight organics are of paramount importance.

The objective of this paper is to systematically investigate the influence of colloidal fouling on trace organic rejection behavior in RO separation. It is hypothesized that cake-enhanced concentration polarization (or osmotic pressure) not only causes a severe permeate flux decline, but also a concomitant decline in the rejection of trace organic compounds. In this investigation, two laboratory-scale crossflow membrane filtration systems were designed specifically to study the influence of crossflow hydrodynamics on the rejection behavior of trace organics by RO membranes in the presence of colloidal fouling. Measurement of colloidal deposit layer mass buildup revealed the role of channel wall shear rate on membrane colloidal fouling and its impact on trace organic rejection.

2. Materials and methods

2.1. Model colloidal particles and membrane

The colloidal silica particles used were provided in aqueous solution by Nissan Chemical Industries (Tarrytown, NY). The particles, denoted MP-3040 by the manufacturer, have a diameter of $0.3 \pm 0.02 \mu\text{m}$. Chemical analysis by the manufacturer specifies the suspension to be 40 wt.% SiO_2 , less than 0.6 wt.% Na_2O , and with a specific gravity of 1.29–1.32 at 20°C . Based on a mean specific gravity of 1.31 and 40 wt.% SiO_2 , the density of the silica particles was calculated to be 2.41 g/cm^3 . By gravimetric analysis, we found that the particle density was 2.15 g/cm^3 .

The RO membrane used in this investigation was a commercially available thin-film composite membrane (LFC-1, Hydranautics, Oceanside, CA). The flat sheet membrane was cut into coupons of size required by the membrane filtration cells, stored in deionized (DI) water (Nanopure Infinity Ultrapure, Barnstead, Dubuque, IA) at about 5°C , with DI water being replaced regularly. The intrinsic physical and chemical properties of this membrane have been characterized extensively in our previous studies [27].

2.2. Organics

2.2.1. Model inert organics

Four inert, neutrally charged model organic compounds were used – two with molecular weight (MW) lesser than 100 g/mol and two with MW greater than 100 g/mol . The

organics with MW lower than 100 g/mol were ethylene glycol (62.1 g/mol) (Product No. 9300; J.T. Baker, Phillipsburg, NJ) and glycerol (92.1 g/mol) (Product No. 2136; J.T. Baker, Phillipsburg, NJ). The two organics with MW greater than 100 g/mol were erythritol (122.2 g/mol) (Product No. E7500; Sigma–Aldrich, St. Louis, MO) and xylose (150.1 g/mol) (Product No. X1500; Sigma–Aldrich, St. Louis, MO).

2.2.2. Model trace organic contaminants

Two types of trace organic contaminants were used for this investigation. They were both radioactive-labeled natural steroid hormones, namely estradiol-2,4-³H (Product No. E9767; Sigma–Aldrich, St. Louis, MO) and (1,2,6,7-³H[N])progesterone (Product No. P5050; Sigma–Aldrich, St. Louis, MO). Both hormones have purity of about 95% and were supplied in ethanol solution. Specific activities of the estradiol and progesterone were 16.8 and 88.0 Ci/mmol, respectively. The hormones were stored in the dark at temperature <4 °C.

2.3. Analysis of organics

A total organic carbon (TOC) analyzer (Shimadzu TOC-Vcsh) was used to analyze the inert organic solute concentration in the feed water and permeate. To prevent colloidal clogging of the combustion column of the carbon analyzer, samples from the feed (10 mL) were filtered with Millex®-GV syringe-driven sterilizing filter unit with a low protein binding, 0.22 µm Durapore (PVDF) membrane (Product No. SLGVR25LS; Millipore, Ireland) prior to TOC analysis. To ensure accuracy of TOC measurement, the carbon analyzer catalyst was frequently changed and the analyzer recalibrated to avoid analytical error due to catalyst clogging by NaCl crystals.

For the radioactive-labeled natural steroid hormones, a liquid scintillation analyzer (Tri-Carb 2900 TR; Packard Instrument Company, Inc., Downers Grove, IL) was used. Hormone concentration in the sample was quantified by first transferring 1 mL of the sample into a scintillation vial, followed by addition of 9 mL of Ultima Gold™ scintillation cocktail (Product No. 6013329; Packard Bioscience Company, Meriden, CT). The vial was then shaken vigorously to ensure that the mixture was mixed uniformly before being transferred to the scintillation analyzer for radioactive counting (5 min counting time). The hormone concentration in the sample was determined by comparing its radioactive reading (in unit of count per minute) with a calibration curve generated at concentrations of 0, 0.01, 0.1, 1, 10, 100 and 1000 ng/L. With this method, the detection limits were approximately 0.5 and 0.1–0.2 ng/L for estradiol and progesterone, respectively.

2.4. Crossflow membrane filtration systems

Two sets of laboratory-scale crossflow membrane filtration systems were used. Fig. 1 shows the schematic diagram of one of the filtration systems. Both systems were identical except the membrane cells – one has a channel height (H_c)

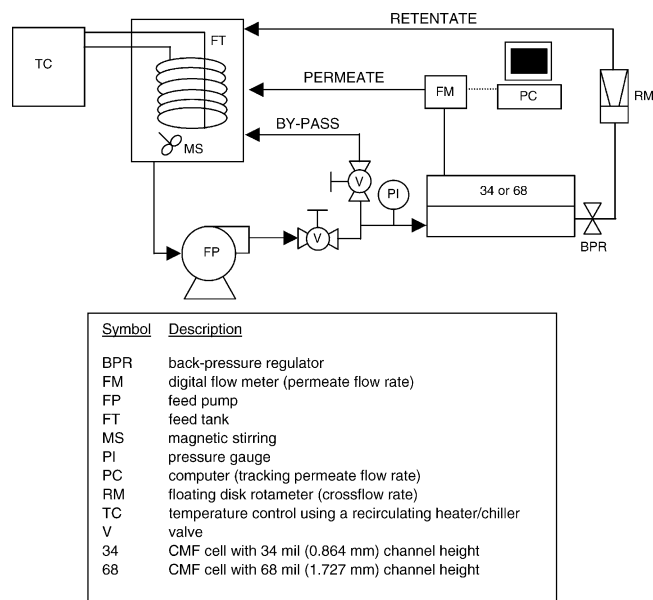


Fig. 1. Schematic diagram of the two membrane filtration units used in the fouling experiments. Both units are identical except the membrane cells – one has a channel height (H_c) of 34 mil (0.86 mm) while the other is 68 mil (1.73 mm).

of 34 mil (0.86 mm) while the other is 68 mil (1.73 mm). The crossflow filtration units will hereafter simply be denoted as the “34” and “68” units, indicating their respective channel heights. Both filtration units were commercially available stainless-steel crossflow membrane filtration systems (CMF) units (Sepa CF, Osmonics Inc., Minnetonka, MN). Both crossflow filtration units have similar dimensions of 14.6 and 9.5 cm for channel length (L_c) and width (W_c), respectively. Thus, each unit has an effective membrane area (A_m) of $1.30 \times 10^{-2} \text{ m}^2$, and cross-sectional flow areas (A_x) of $0.82 \times 10^{-4} \text{ m}^2$ for the 34 unit and $1.64 \times 10^{-4} \text{ m}^2$ for the 68 unit.

Feed was delivered to the Sepa CF cell using a 6.83 L/min (1.8 gpm) constant flow diaphragm pump (Hydra-Cell M-03; Wanner Engineering, Inc., Minneapolis, MN). The feed suspension was fed from a 20-L magnetically stirred high-density polyethylene reservoir having a feed water volume of 10 L. An immersed stainless-steel coil with water fed from a refrigerated bath/circulator (Model No. RTE-111; Thermo NESLAB, Portsmouth, NH) was used to maintain the feed water temperature at 20 ± 0.5 °C. The retentate flow rate was monitored by a variable area flow meter (Model No. F-40375LN-8; Blue-White Industries, Ltd., Huntington Beach, CA). Applied pressure, monitored by a pressure gauge (Model No. PG10000; PSI-Tronix, Inc., Tulane, CA) at the channel inlet, was controlled by a bypass needle valve (Product No. 4M-V4LR-SS; Parker Hannifin Corp., Jacksonville, AL) at the channel inlet and a back-pressure regulator (Model No. 13020; US Paraplate Corp., Sacramento, CA) at the channel outlet. This combination allowed fine control of applied pressure and crossflow velocity. A digital flow meter (Opti-flow 1000; Agilent Technologies, Palo Alto, CA), interfaced

with a personal computer, was used to continuously monitor the permeate flux. During filtration, permeate and retentate were recycled back into the feed tank.

2.5. Membrane fouling

The experimental protocol for the colloidal fouling experiments involved the following steps: (1) equilibration of the membrane with 10 L of DI water for 24 h at 250 psi (1724 kPa); (2) addition of 200 mL of 5 M NaCl stock solution into the feed tank to achieve a 50 mM NaCl concentration; (3) adjustment of the applied pressure to achieve a permeate flux of 1.42×10^{-5} m/s (30 gfd) and equilibration for another 6 h; (4) addition into the feed tank of either inert organics of interest to achieve an initial TOC concentration of 45.0 ± 1.1 mg/L, or a hormone of interest to achieve an initial hormone concentration of 100 ng/L, followed by further equilibration for 0.5 h; and (5) commencement of accelerated fouling run by adding colloidal stock solution into the feed tank to achieve an initial feed particle concentration of 200 mg/L.

For the fouling experiments, grab samples of feed and permeate were taken at the start, at the end, and at several predetermined time intervals during the fouling experiment. Samples were analyzed for conductivity, either TOC or hormone concentration, turbidity, and pH to monitor salt and either organic or hormone rejection, and cake layer mass.

2.5.1. Membrane filtration system cleaning

After each fouling experiment, rigorous cleaning of the filtration units was carried out to remove colloidal particles remained in the system. The cleaning procedure involved the following steps: (1) the feedwater was emptied after the fouling experiment; (2) the fouled membrane coupon was replaced by a fresh membrane coupon; (3) the filtration unit was operated for 1 h with DI water adjusted to pH 11 at temperature of 30 °C and applied pressure of 150 psi (1034 kPa); (4) the feedwater was replaced with DI water (unadjusted pH) and filtration was resumed for 1 h at temperature of 20 °C and applied pressure of 150 psi; and (5) step (4) was repeated for additional three times.

2.5.2. Membrane hydraulic resistance measurement

After membrane compaction and prior to each fouling experiment, when stable flux was achieved, the RO membrane hydraulic resistance was determined by measuring pure water flux over a range of applied pressure. The pressure range tested was 345–1724 kPa (50–250 psi) and the retentate crossflow velocity was 9.6 cm/s. Details on this procedure can be found elsewhere [7].

2.5.3. Experimental conditions

Table 1 summarizes the operating conditions of the fouling experiments. Crossflow velocities ranging from 9.6 to 53.8 cm/s were used, which resulted in initial channel wall shear rates ranging from 333 to 3736 s⁻¹. The volume of feed

Table 1
Operating conditions for fouling experiments

RO unit	Q (Lpm)	J_0 (m/s)	u (cm/s) ^a	Initial γ_0 (s ⁻¹) ^b	Initial Re (-) ^c
68	0.95	1.42×10^{-5}	9.6	333	363
34	0.95	1.42×10^{-5}	19.2	1334	363
68	1.89	1.42×10^{-5}	19.2	666	727
34	1.89	1.42×10^{-5}	38.4	2669	727
68	2.65	1.42×10^{-5}	26.9	932	1018
34	2.65	1.42×10^{-5}	53.8	3736	1018

The variables are as follows: Q is the volumetric feed flow rate (given in liter per minute), J_0 the initial flux, u the crossflow velocity, γ_0 the initial shear rate, and Re is the Reynolds number.

^a $u = Q/A_x$, where A_x is the channel cross-sectional area.

^b $\gamma_0 = 6u/H_c$, with H_c being the channel height.

^c $Re = ud_h/\nu$, with ν being the kinematic viscosity and the hydraulic diameter $d_h = 2H_c$.

water was 10 L and its pH was 6.8 ± 0.2 throughout the fouling experiments. For all fouling experiments, the initial flux was set at 1.42×10^{-5} m/s (30 gfd) by adjusting the applied pressure, which was 323 ± 22 and 301 ± 20 psi for the 68 and 34 units, respectively.

2.5.4. Measurement of deposited particle mass

Samples of feed water and permeate were collected at the start, the end, and several predetermined time intervals for turbidity measurement (Model 2100N Turbidimeter; Hach Company, Loveland, CO) to determine the cake layer buildup during the fouling experiment. The corresponding mass of the particles deposited on the membrane surface was calculated from a mass balance based on the change in feed water turbidity as fouling progressed [5].

2.6. Calculation of cake-enhanced osmotic pressure

The cake-enhanced osmotic pressure for the fouling experiments was calculated based on a modified hindered mass transfer coefficient and the cake-enhanced osmotic pressure model originally developed by Hoek et al. [7]. The calculations considered only the effects of NaCl since its concentration (50 mM or 2925 mg/L) was much higher than the concentration of organics. The cake-enhanced osmotic pressure was calculated for each sampling point during the experiment by using the required experimentally measured parameters in the model. The following subsections describe briefly the model and Fig. 2 summarizes the steps in calculating the cake-enhanced osmotic pressure.

2.6.1. Governing equations for “cake-enhanced” osmotic pressure

The modified transient flux is described by [7]

$$J(t) = \frac{\Delta P - \Delta\pi_{m1}^*(t)}{\mu[(R_m + R_c(t))]} \quad (1)$$

where J is the permeate flux, ΔP the applied pressure, $\Delta\pi_{m1}^*$ the cake-enhanced osmotic pressure, μ the solvent viscosity,

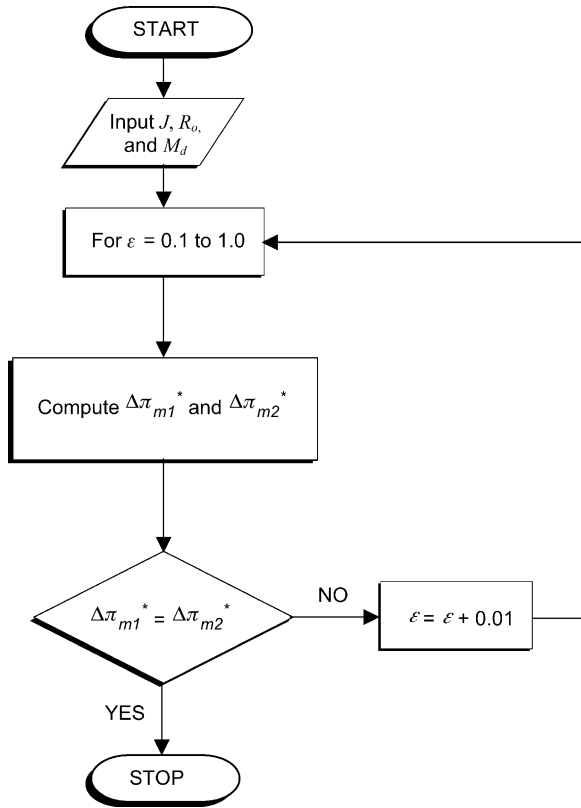


Fig. 2. A recursive algorithm for solving the cake-enhanced osmotic pressure at each sampling point of the fouling experiment (modified from the model developed by Hoek et al. [7]).

R_m the membrane hydraulic resistance, and R_c the cake layer resistance, which is defined as [5]

$$R_c(t) = \alpha M_d(t) = \left[\frac{180(1 - \varepsilon(t))}{\rho_p d_p^2 \varepsilon(t)^3} \right] M_d(t) \quad (2)$$

Here, α is the specific cake resistance, M_d the transient deposit layer mass per unit membrane area, ε the cake layer porosity, ρ_p the particle density, and d_p the particle diameter.

Rearrangement of Eq. (1) after substitution of R_c from Eq. (2) yields the first equation describing the cake-enhanced osmotic pressure:

$$\Delta\pi_{m1}^*(t) = \Delta P - J(t)\mu R_m - \mu J(t) \frac{180(1 - \varepsilon(t))}{\rho_p d_p^2 \varepsilon(t)^3} M_d(t) \quad (3)$$

The second equation which describes the cake-enhanced osmotic pressure is developed from a steady-state mass balance in the CP layer and the van't Hoff's law. The solvent flux is governed by the following one-dimensional steady-state mass balance across the CP layer:

$$JC - D \frac{dC}{dy} = JC_p \quad (4)$$

where C is the NaCl concentration, C_p the permeate NaCl concentration, D the NaCl diffusivity in the bulk, and y the

distance perpendicular to and away from the membrane surface [28].

Integration of Eq. (4) over the salt concentration polarization layer thickness (δ) with the appropriate boundary conditions (i.e., $C = C_m$ at $y = 0$ and $C = C_b$ at $y = \delta$) and substitution into van't Hoff's law yields the second equation which describes the cake-enhanced osmotic pressure:

$$\Delta\pi_{m2}^*(t) = 2C_b R T R_o(t) \exp\left(\frac{J(t)}{k^*(t)}\right) \quad (5)$$

where C_b is the bulk NaCl molar concentration, R the universal gas constant, T the absolute temperature, R_o the observed NaCl rejection, and k^* the "hindered" mass transfer coefficient, which its estimation is discussed in detail in Section 3.2.

3. Results and discussion

3.1. Colloidal cake layer buildup and flux decline

The mass of silica colloids deposited on the membrane surface for the different hydrodynamic conditions shown in Table 1 is plotted as a function of time in Fig. 3. In general, the deposited mass on the membrane increased rapidly initially, but subsequently slowed down and approached a maximum value. During the first approximately 20 h, the amounts of colloids deposited were almost the same, despite different channel wall shear rates. This suggests that an initial period of time exists for which crossflow hydrodynamics do not affect significantly the deposition of colloids. At later stages, the rate of colloid accumulation on the membrane surface decreased with increasing channel wall shear rate. This observation is expected since it is typically assumed that the shear rate limits cake growth in crossflow membrane

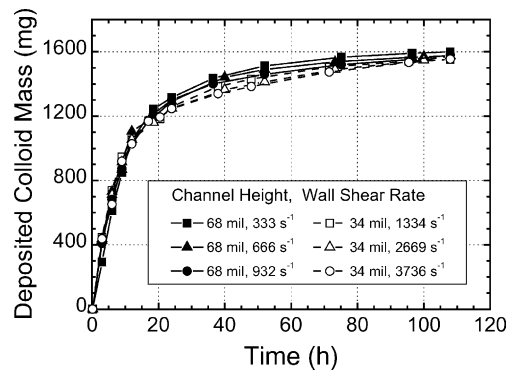


Fig. 3. Mass of colloids deposited on the membrane surface as a function of time for the experimental conditions shown in Table 1. Closed symbols represent data obtained from the 68 unit and open symbols represent data from the 34 unit. The corresponding crossflow channel heights and wall shear rates are summarized in the figure keys. Other experimental conditions were: initial permeate flux = 1.42×10^{-5} m/s (30 gfd), ionic strength = 50 mM NaCl, initial feed colloid concentration = 200 mg/L, temperature = 20 °C, and pH = 6.8.

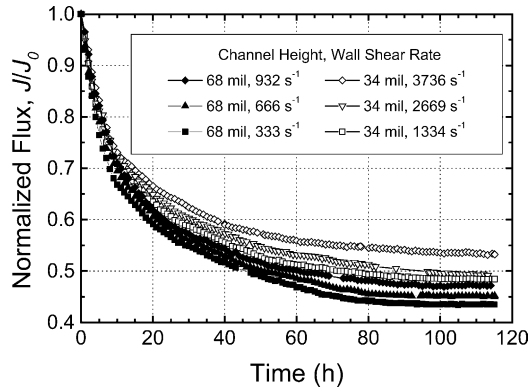


Fig. 4. Normalized flux decline data vs. time during the fouling experiments under the conditions shown in Table 1. Channel heights and wall shear rates are indicated in the figure keys. Other experimental conditions were: initial permeate flux = 1.42×10^{-5} m/s (30 gfd), ionic strength = 50 mM NaCl, initial feed colloid concentration = 200 mg/L, temperature = 20 °C, and pH = 6.8.

filtration [29]. Similar observations were also reported by Hoek et al. [7].

Normalized flux (J/J_0) data as a function of time are plotted in Fig. 4. In all experimental conditions, permeate flux started to decline as soon as colloids were introduced. After the colloidal deposition rate had stabilized, permeate flux started to stabilize as well. For the first 4 h of the fouling experiments, permeate fluxes for all runs were almost similar regardless of channel height and channel wall shear rate. At the later stage, the rate of flux decline was directly related to the channel wall shear rate. At higher channel wall shear rates, lesser mass of colloids was deposited and, hence, permeate flux was higher.

3.2. Cake-enhanced osmotic pressure

The transient trans-membrane pressure ($\Delta P_m = J\mu R_m$), the transient cake-enhanced osmotic pressure ($\Delta\pi_m^*$), and the transient trans-cake hydraulic pressure (ΔP_c) were computed at each sampling point. Since the NaCl molar concentration in the feed water was several orders of magnitudes higher than the concentration of the organics used, the polarization layer developed during the fouling experiment was primarily due to NaCl. Hence, the calculations were based on NaCl experimental data. Calculation of the osmotic pressure due to membrane fouling was generally based on the cake-enhanced osmotic pressure model of Hoek et al. [7,30]. Slight modifications were made to the original model to account for the thick cake layer formed on the membrane surface as described below.

Since almost all the colloids present in the feed (200 mg/L) were deposited on the membrane surface by the end of the fouling runs, the developed cake layer was thick enough to increase the crossflow shear rate when the membrane was fouled significantly by colloids. Consequently, the mass transfer coefficient (from film theory), k_f , and the NaCl concentration polarization (film) layer thickness, δ_f , are no longer

constants. The mass transfer coefficient k_f is determined at each point of the experiment using [31]:

$$k_f(t) = 1.62 \left(\frac{\gamma_0(t) D^2}{12 L_c} \right)^{1/3} \quad (6)$$

where L_c is the channel length and γ_0 the channel wall shear rate at each point of the experiment.

In the calculation of the effective shear rate, γ_0 , the cake layer thickness, δ_c , was taken into account to determine the effective channel height, $H_c(t)$. The cake layer thickness was estimated from the transient deposit layer mass per unit membrane area, M_d [5]:

$$\delta_c(t) = \frac{M_d(t)}{\rho_p(1 - \varepsilon(t))} \quad (7a)$$

$$H_c(t) = H_{c0} - \delta_c(t) \quad (7b)$$

where H_{c0} is the cell channel height. Thus, knowing $H_c(t)$ allows the calculation of the shear rate [29]:

$$\gamma_0(t) = \frac{6u(t)}{H_c(t)} \quad (8)$$

using the available channel cross-sectional area for crossflow, $A_x(t)$, and the crossflow velocity, $u(t)$:

$$A_x(t) = W_c H_c(t) \quad (9a)$$

$$u(t) = \frac{Q}{A_x(t)} \quad (9b)$$

Here, W_c is the channel width and Q the volumetric crossflow rate. From the calculated $k_f(t)$ (Eq. (6)), the NaCl concentration polarization (film) layer thickness, δ_f , is determined from

$$\delta_f(t) = \frac{D}{k_f(t)} \quad (10)$$

The “hindered” mass transfer coefficient, k^* , is comprised of two parts – one describing mass transfer between the membrane surface and colloidal cake layer, and one describing mass transfer between the interface of the colloidal cake layer and the bulk solution:

$$\frac{1}{k^*(t)} = \frac{\delta_c(t)}{D^*(t)} + \frac{\delta_s(t)}{D} \quad (11)$$

where δ_c is the cake layer thickness, δ_s the difference between the film (δ_f) and cake layer thickness (since the film thickness is assumed constant), and D^* the hindered diffusion coefficient. The hindered diffusion coefficient, D^* , is dependent on porosity and diffusive tortuosity ($\tau \approx 1 - \ln \varepsilon^2$) [32] and is estimated as

$$D^* = \left(\frac{\varepsilon}{\tau} \right) D = \left(\frac{\varepsilon}{1 - \ln \varepsilon^2} \right) D \quad (12)$$

During the initial stage of colloidal fouling, the cake layer thickness is thin compared to the salt film-layer thickness. With the mass transfer coefficient, $k_f = D/\delta_f$, rearrangement of Eq. (11) yields the hindered mass transfer coefficient, k^* ,

which is applicable when the cake layer thickness is thin (i.e., $\delta_c < \delta_f$):

$$\frac{1}{k^*(t)} = \delta_c(t) \left(\frac{1 - \ln \varepsilon(t)^2}{\varepsilon(t)D} - \frac{1}{D} \right) + \frac{1}{k_f(t)} \quad (13)$$

However, when the colloidal cake layer thickness becomes thicker (i.e., $\delta_c > \delta_f$), the salt film-layer thickness that extends from the interface of the colloidal cake layer to the bulk can be assumed negligible (i.e., $\delta_s \approx 0$), since the mass transfer is mainly controlled by the colloidal cake layer. Hence, the hindered mass transfer coefficient is simplified to

$$\frac{1}{k^*(t)} = \frac{\delta_c(t)}{D^*(t)} \quad (14)$$

The applied pressure as well as the calculated transient trans-membrane pressure (ΔP_m), the transient cake-enhanced osmotic pressure ($\Delta \pi_m^*$), and the transient trans-cake hydraulic pressure (ΔP_c) for the experiments described earlier are shown in Fig. 5. The latter pressures were calculated from the revised method described above and the algorithm shown in Fig. 2. To achieve an initial permeate flux of 1.42×10^{-5} m/s (30 gfd), the required applied pressure ranged from about 282 to 352 psi, depending on the crossflow velocity and channel height. A lower crossflow velocity and a higher channel height required higher applied pressure to achieve the same initial permeate flux, since the wall shear rate is lower and the concentration polarization is more severe. As the membrane was fouled, the transient trans-membrane pressure (ΔP_m) decreased, the transient cake-enhanced osmotic pressure ($\Delta \pi_m^*$) increased, and the transient trans-cake hydraulic pressure (ΔP_c) increased. All these pressures approached stabilized values after all the colloids in the feed were deposited on the membrane surface. The results clearly show that flux decline is caused primarily by the elevated transient cake-enhanced osmotic pressure ($\Delta \pi_m^*$) – a direct consequence of the cake-enhanced concentration polarization. As previously suggested [7,30], the trans-cake hydraulic resistance (or pressure) has a negligible effect on flux decline.

3.3. Salt rejection due to colloidal fouling

Fig. 6 presents the salt rejection profiles for different cross-flow hydrodynamic conditions. From this plot with a magnified scale (observed rejection ranges from 86 to 100%), we observed that salt rejection in all cases decreased to a minimum at around 40 h, then improved slightly, and subsequently stabilized. The recovery in salt rejection occurred approximately from the point when the permeate water flux stabilized. Furthermore, this phenomenon was observed as the ratio of the permeate flux to the hindered mass transfer coefficient, J/k^* , stabilized (Fig. 7).

To investigate whether this phenomenon was caused by the cake layer deposited on the membrane, two additional experiments were carried out using: (1) NaCl feed concentration of

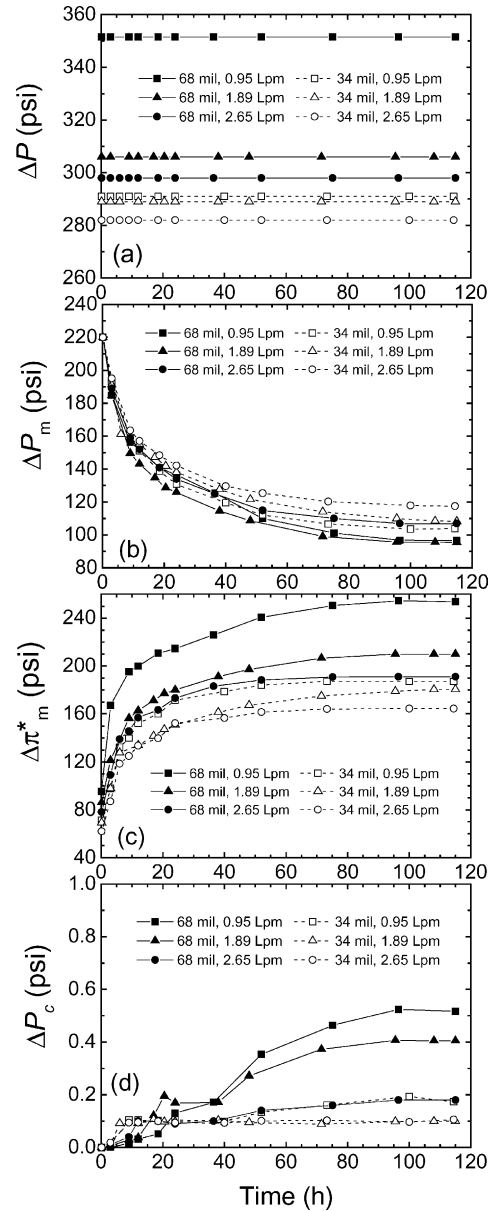


Fig. 5. Variation as a function of time of (a) applied pressure (ΔP), (b) calculated trans-membrane pressure drop (ΔP_m), (c) cake-enhanced osmotic pressure ($\Delta \pi_m^*$), and (d) trans-cake pressure drop (ΔP_c). Data are for the experiments shown in Figs. 3 and 4.

50 mM without any colloids and (2) NaCl feed concentration of 50 mM with an initial feed colloid concentration of only 40 mg/L. Both experiments were carried out in the 68 unit cell at a retentate crossflow velocity of 9.6 cm/s (0.95 Lpm). The observed salt rejections obtained from these two experiments are shown in Fig. 8. The results show that salt rejection improved slightly with time during the experiment without colloids. For the test with an initial feed colloidal concentration of 40 mg/L, the observed salt rejection reduced slightly but increased after 10 h. At 115 h, the observed salt rejection was 97%, slightly higher than the initial ($t = 0$) observed salt rejection of 96.5%.

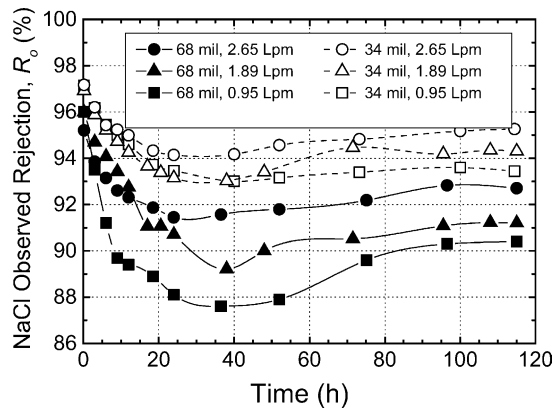


Fig. 6. Observed salt rejection (R_o) as a function of time for the fouling experiments shown in Figs. 3 and 4. Experimental conditions were: initial permeate flux = 1.42×10^{-5} m/s (30 gfd), ionic strength = 50 mM NaCl, initial feed colloid concentration = 200 mg/L, temperature = 20 °C, and pH = 6.8.

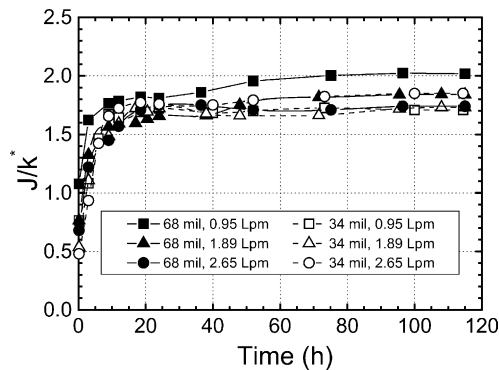


Fig. 7. Variation of the ratio of permeate flux to hindered mass transfer coefficient (J/k^*) as a function of time for the fouling experiments shown in Fig. 4.

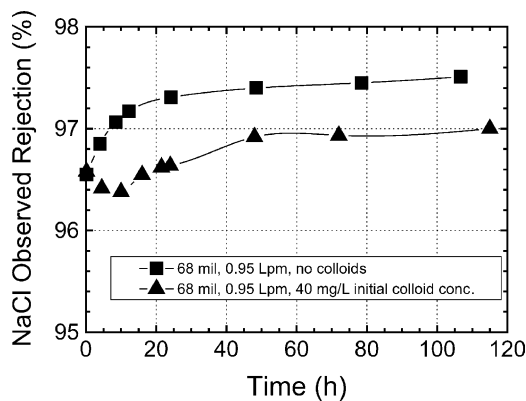


Fig. 8. Observed salt rejection (R_o) as a function of time for experiments with colloid-free solution and with 40 mg/L initial feed colloid concentration. Similar test conditions were employed in both experiments: 68 unit ($H_c = 1.73$ mm), ionic strength = 50 mM NaCl, crossflow velocity $u = 9.6$ cm/s ($Q = 0.95$ Lpm), $J_0 = 1.42 \times 10^{-5}$ m/s (30 gfd), temperature = 20 °C, and pH = 6.8.

Comparing the results between experiments with initial colloid concentration of 40 and 200 mg/L at the same hydrodynamic conditions, salt rejection declined much less than in the case with higher (200 mg/L) colloid concentration, and the minimum in salt rejection occurred earlier, at about 10 h rather than 40 h. Salt rejection decline was lower for the case with lesser initial colloid concentration because lower mass of colloids was deposited on the membrane, which, in turn, imposed lesser back diffusion hindrance of solute from the membrane surface to the bulk solution. The normalized flux decline and cake layer buildup for the experiment with 40 mg/L particles are shown in Fig. 9. Similar to the previous experiments, the flux decreased as colloids were introduced and it stabilized after most of the colloids were deposited on the membrane. Results from these experiments suggest that the improvement in salt rejection as the system stabilized (complete deposition of colloids) was not primarily due to the cake layer buildup. Instead, it was a phenomenon due to the intrinsic behavior of the RO membrane – that is, as flux and diffusion rate stabilized, salt rejection improves slightly with time.

The observation that salt rejection declined significantly with colloidal fouling confirmed our hypothesis that the buildup of cake layer at the membrane surface hinders back diffusion of solute from the membrane surface to the bulk solution. The increase in salt concentration at the membrane surface creates greater salt concentration gradient across the membrane, causing an increase in permeate salt concentration and a decrease in observed salt rejection by the RO membrane. The extent of observed salt rejection decline and the stabilized value due to colloidal fouling appeared directly related to the channel wall shear rate. Even though the colloidal deposition rates were almost identical (Fig. 3) for all hydrodynamic conditions during the first ca. 20 h, the decline in observed salt rejection was higher at lower channel wall shear rates. This suggests the dominating effect of channel wall shear rate on concentration polarization layer thickness

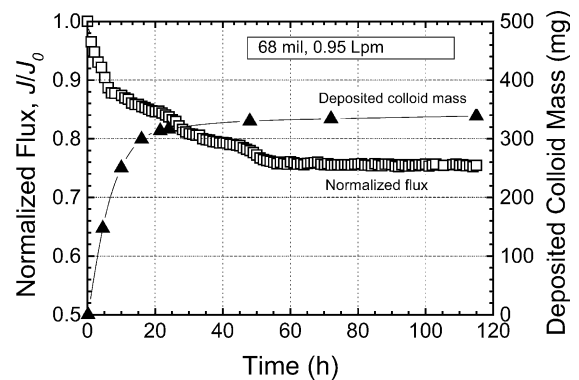


Fig. 9. Normalized flux and mass of colloids deposited on the membrane as a function of time for the experiments with 40 mg/L initial feed colloid concentration. A constant feed flow rate of 0.95 Lpm provided an initial shear rate of 333 s^{-1} in the 68 unit ($H_c = 1.73$ mm). Other experimental conditions were: $J_0 = 1.42 \times 10^{-5}$ m/s (30 gfd), temperature = 20 °C, ionic strength = 50 mM NaCl, and pH = 6.8.

and the consequent buildup of cake-enhanced osmotic pressure during the initial stages of colloidal fouling.

3.4. Rejection of inert organic solutes

The predominant rejection mechanisms of small organic molecules by RO membranes are steric interaction, charge exclusion (repulsion), and adsorption to the membrane surface [9–15,33,34]. The inert organic compounds used in this study were neutrally charged and their adsorption to the membrane surface is negligible. Thus, the inert organics and the RO membrane have no charge interaction and adsorptive effects. The primary mechanism for their removal by RO membranes is size (or steric) exclusion [33].

The concentrations of the organics in the feed and permeate were measured during the experiments. Their feed concentrations were found to be almost constant throughout the fouling runs, suggesting that degradation or volatilization of organics did not occur during the relatively long period of experiments. Figs. 10–12 present the observed rejections of the model organics (ethylene glycol, glycerol, xylose, and erythritol). The results show that the rejection of neutrally charged organics by the RO membrane is strongly related to their molecular weights. Organics with MW lower than about 100 g/mol had a lower initial observed rejection and a larger decrease in the observed rejection as the membrane was fouled (Figs. 10 and 11). For example, the initial observed rejection and the decrease in observed rejection (stabilized observed rejection minus initial observed rejection) due to fouling for ethylene glycol (62.1 g/mol) were about 64 and 31%, respectively (Fig. 10). In comparison, the initial observed rejection and the decrease in observed rejection for glycerol (92.1 g/mol) were about 91 and 8%, respectively (Fig. 11). For both ethylene glycol and glycerol, observed rejections showed similar behavior as the salt rejection during membrane fouling – organic rejection decreased

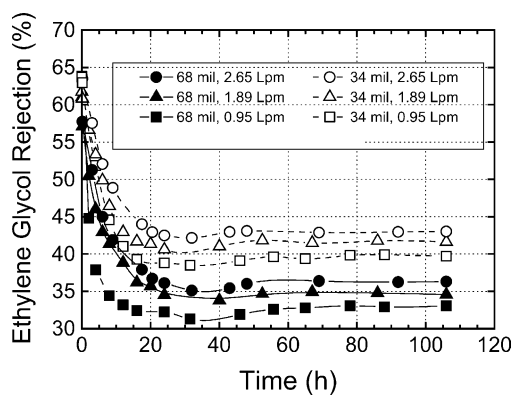


Fig. 10. Ethylene glycol observed rejection as a function of time for the experimental conditions shown in Table 1. Experiments were conducted at constant physico-chemical conditions: feed ethylene glycol concentration = 45 mg/L (as TOC), initial permeate flux = 1.42×10^{-5} m/s (30 gfd), ionic strength = 50 mM NaCl, initial feed colloid concentration = 200 mg/L, temperature = 20 °C, and pH = 6.8.

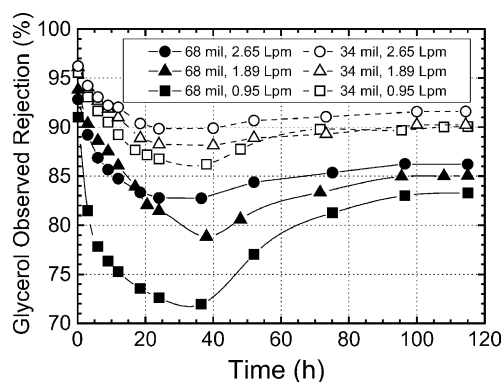


Fig. 11. Glycerol observed rejections as a function of time for the experimental conditions shown in Table 1. Experiments were conducted at constant physico-chemical conditions: feed glycerol concentration = 45 mg/L (as TOC), initial permeate flux = 1.42×10^{-5} m/s (30 gfd), ionic strength = 50 mM NaCl, initial feed colloid concentration = 200 mg/L, temperature = 20 °C, and pH = 6.8.

to a minimum, improved slightly, and stabilized subsequently.

For organics with MW larger than about 100 g/mol, the colloidal cake layer did not affect much the subsequent organic rejection (Fig. 12). The results show that the observed rejection of xylose (150.1 g/mol) decreased slightly with time, whereas observed rejection of erythritol (122.2 g/mol) decreased slightly more as the membrane was fouled. For “large” MW organics, fouling did not result in a decrease in rejection because the primary mechanism for rejection of such organics by the RO membrane was size exclusion. Even though the cake layer hindered the back diffusion of these organics from the membrane surface to the bulk solution, which constituted to a buildup of a higher organic concentration at the membrane surface, effective retention of these large MW organics by the RO membrane allowed their rejection to remain almost constant.

The observation that low MW organics (MW < 100 g/mol) declined significantly as the membrane was fouled confirmed

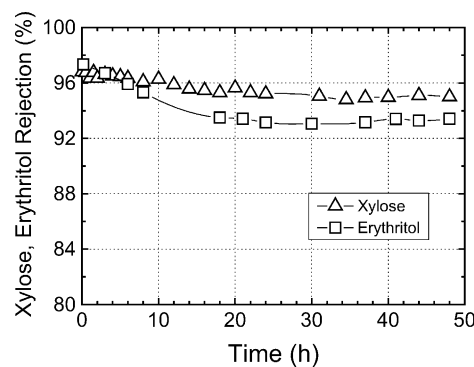


Fig. 12. Xylose and erythritol observed rejections as a function of time. Test conditions employed were: 68 unit ($H_c = 1.73$ mm), crossflow velocity = 9.6 cm/s ($Q = 0.95$ Lpm), feed xylose or erythritol concentration = 45 mg/L (as TOC), initial permeate flux = 1.42×10^{-5} m/s (30 gfd), ionic strength = 50 mM NaCl, initial feed colloid concentration = 200 mg/L, temperature = 20 °C, and pH = 6.8.

our hypothesis that the buildup of cake layer at the membrane surface not only hindered back diffusion of salt from the membrane surface to the bulk solution, but also of low MW organics. Similarly to NaCl, the extent of decline in observed rejection of organics due to colloidal fouling appeared directly related to the channel wall shear rate. At higher channel wall shear rate, the stabilized observed organic rejection was higher and the difference between the stabilized and the minimum observed rejection was smaller.

3.5. Rejection of natural hormones

Removal of radioactive-labeled steroid hormones – progesterone and estradiol – by the RO membrane was studied with and without colloidal fouling. The concentrations of radioactive-labeled progesterone and estradiol in the feed and permeate were measured during the fouling experiments and the results are presented in Fig. 13. In contrast to the model organics discussed earlier, progesterone and estradiol concentrations in the feed were observed to decrease continuously throughout the experiments. Furthermore, during fouling the progesterone and estradiol concentrations in the permeate increased and stabilized at around 40 h. The permeate concentration of both progesterone and estradiol followed a breakthrough curve typically observed in activated carbon adsorption or ion exchange. The stabilized permeate concentration of progesterone was relatively lower (about 6 ng/L) compared to that of estradiol (about 15 ng/L).

The observed continual decrease of hormones in the feed is attributed to adsorption of hormones on the polyamide RO membrane. Previous studies have shown that natural hormones can adsorb or partition into the membrane polymer extensively [34,35]. As the adsorption of hormones to the membrane reaches equilibrium, their feed concentrations stabilize as observed by the smaller rate of decline in hormone feed

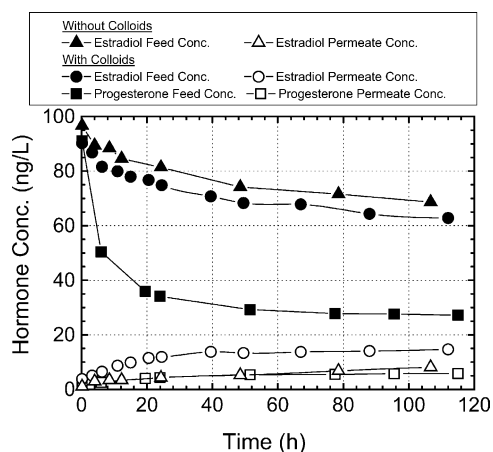


Fig. 13. Progesterone and estradiol concentrations in the feed and permeate as a function of time. Test conditions employed were: 68 unit ($H_c = 1.73$ mm), crossflow velocity = 9.6 cm/s ($Q = 0.95$ Lpm), initial feed progesterone or estradiol concentration = 100 ng/L, initial permeate flux = 1.42×10^{-5} m/s (30 gfd), ionic strength = 50 mM NaCl, initial feed colloid concentration = 200 mg/L, temperature = 20 °C, and pH = 6.8.

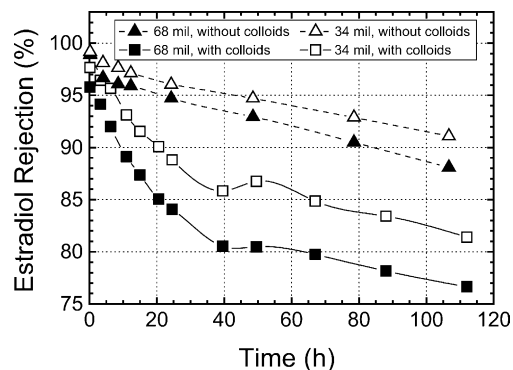


Fig. 14. Estradiol observed rejection as a function of time for runs with 200 mg/L initial feed colloid concentration and runs with colloid-free solution. Experiments were conducted with the 68 ($H_c = 1.73$ mm) and 34 ($H_c = 0.864$ mm) units at a total flow rate $Q = 0.95$ Lpm. Test conditions employed were: initial crossflow velocities of 9.6 and 19.2 cm/s for the 68 and 34 units, respectively, initial feed estradiol concentration = 100 ng/L, initial permeate flux = 1.42×10^{-5} m/s (30 gfd), ionic strength = 50 mM NaCl, temperature = 20 °C, and pH = 6.8.

concentration at the later stages of the experiments (Fig. 13). Progesterone concentration in the feed was observed to decrease rapidly during the first 20 h of the fouling experiment but declined slowly subsequently. In contrast, the concentration of estradiol in the feed declines gradually throughout the experiments regardless of fouling or not. This may be attributed to progesterone adsorbing onto the membrane polymer at a faster rate since it has a higher octanol–water partition coefficient ($\log K_{ow}$) than estradiol (4.63 compared to 4.01).

The observed rejection behavior of estradiol for both fouling and non-fouling experiments is shown in Fig. 14. For the runs without colloidal fouling, the decrease in observed estradiol rejection appeared to be linear, whereas for the case with colloidal fouling, the observed rejection decreased sharply in the first 40 h, followed by a moderate linear decline. In addition, the decrease in observed estradiol rejection was more severe with colloidal fouling. At the end of the experiments, the decrease in observed estradiol rejection was about 18% with colloidal fouling, compared to about 10% without colloidal fouling, for the experiments conducted with the 68 mil unit at a crossflow velocity of 9.6 cm/s (0.95 Lpm). As for the test with the 34 mil unit, the decrease in observed estradiol rejection was about 15% with colloidal fouling and about 7% without colloidal fouling. The reason is similar to the rejection of organics discussed earlier – the cake layer formed on the membrane surface hinders the back diffusion of the estradiol from the membrane surface back to the bulk solution. Consequently, buildup of estradiol on the membrane surface created a larger concentration gradient for its diffusion across the RO membrane.

Fig. 15 depicts the effect of colloidal fouling on the observed rejection of progesterone for two different hydrodynamic conditions. In contrast to estradiol which displayed linear observed rejection decline profiles, progesterone rejection

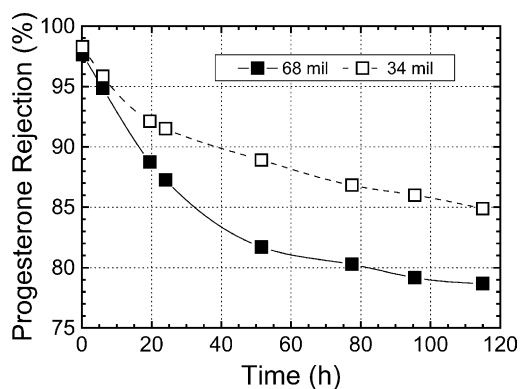


Fig. 15. Progesterone observed rejection as a function of time for runs with 200 mg/L initial feed colloid concentration and runs with colloid-free solution. Experiments were conducted with the 68 ($H_c = 1.73$ mm) and 34 ($H_c = 0.864$ mm) units at a total flow rate $Q = 0.95$ Lpm. Test conditions employed were: initial crossflow velocities of 9.6 and 19.2 cm/s for the 68 and 34 units, respectively, initial feed estradiol concentration = 100 ng/L, initial permeate flux = 1.42×10^{-5} m/s (30 gfd), ionic strength = 50 mM NaCl, temperature = 20 °C, and pH = 6.8.

decreased sharply initially but slowed down gradually until the end of the experiment. After 115 h of colloidal fouling, the decreases in progesterone rejection for the 68 and 34 mil units were about 19 and 13%, respectively. Higher decrease in progesterone and estradiol rejections in the 68 mil unit compared to the 34 mil unit confirmed that higher channel wall shear rate had a lesser deteriorating impact on hormone rejection – a similar observation found for inert organics and salt rejections.

The results in Figs. 14 and 15 show that rejection of progesterone and estradiol continued to decline throughout the fouling experiments, even after most of the colloids had deposited on the membrane surface and the flux had stabilized. This observation was in contrast with the salt and inert organic rejection behavior where the observed rejection declined but improved after about 40 h. The continual decrease of hormone concentration in the feed and the concomitant increase in the permeate hormone concentration indicate that there was another dominating mechanism occurring in the separation of hormones by the RO membrane under both fouling and non-fouling conditions. It is suggested that the adsorbed (partitioned) hormones slowly diffuse through the polymer matrix of the RO membrane and eventually appear in the permeate side. We have recently discussed such a process in the separation of hormones by polymeric nanofiltration membranes [36]. Thus, despite the relatively large molecular weight of hormones (272.4 g/mol for estradiol and 314.5 g/mol for progesterone), their rejection by RO membranes is not complete as with inert organics. The passage of hormones through RO membranes and the severe decline in rejection due to fouling have important implications for advanced water reclamation, as domestic wastewaters contain a myriad of trace organic contaminants, including hormones and other endocrine disrupting chemicals.

4. Concluding remarks

Development of a colloidal cake layer on the membrane surface restricted back diffusion of both salt and inert organic solutes, resulting in significant decline in their rejection. Rejection of low molecular weight organic solutes depended directly on the wall shear rate. Solute rejection was higher at higher wall shear rate, suggesting a thinner concentration polarization layer and a slower buildup of solute concentration at the membrane surface. For larger molecular weight inert organic solutes, steric exclusion controlled their removal and colloidal fouling had a small effect on their rejection. For trace organic contaminants (hormones), colloidal fouling caused a rapid decrease in hormone feed concentration as well as a significant increase in their permeate concentration. In contrast to salt and inert organic solutes, hormone rejection continued to decline even though most of the colloidal particles had deposited on the membrane and the permeate flux had stabilized. This behavior is attributed to the dominating effect of hormone adsorption to the membrane polymeric skin layer and subsequent diffusion of the hormones across the skin layer to the permeate side. It is further suggested that thin-film composite RO membranes are only capable of achieving high retention of hormones at the initial stages of filtration. Rejection deteriorates as adsorbed hormones diffuse through the polymeric membrane matrix to the permeate side. Hormone breakthrough is accelerated significantly under colloidal fouling conditions. Because fouling has a significant impact on permeate water quality, pretreatment for effective removal of potential foulants is a critical step in RO operation to ensure consistent production of high quality water.

Acknowledgements

The authors acknowledge the support by the US National Science Foundation (Grant BES 0114527) and the National University of Singapore Postdoctoral Training Fellowship to H.Y. Ng.

References

- [1] M. Sugahara, T. Kitao, Y. Terashima, S. Iwai, Transport properties of thermally conditioned sludge liquors in reverse osmosis, *Inter. Chem. Eng.* 19 (1979) 322–328.
- [2] B.A. Winfield, A study of the factors affecting the rate of fouling of reverse osmosis membranes treating secondary sewage effluents, *Water Res.* 13 (1979) 565–569.
- [3] R.D. Cohen, R.F. Probstein, Colloidal fouling of reverse osmosis membranes, *J. Colloid Interf. Sci.* 114 (1986) 194–207.
- [4] J. Gilron, D. Hasson, Calcium sulphate fouling of reverse osmosis membrane: flux decline mechanism, *Chem. Eng. Sci.* 42 (1987) 2351–2360.
- [5] R.S. Faibish, M. Elimelech, Y. Cohen, Effect of interparticle electrostatic double layer interactions on permeate flux decline in crossflow membrane filtration of colloidal suspensions: an experimental investigation, *J. Colloid Interf. Sci.* 204 (1998) 77–86.

- [6] S.G. Yiantsios, A.J. Karabelas, The effect of colloid stability on membrane fouling, *Desalination* 118 (1998) 143–152.
- [7] E.M.V. Hoek, A.S. Kim, M. Elimelech, Influence of crossflow membrane filter geometry and shear rate on colloidal fouling in reverse osmosis and nanofiltration separations, *Environ. Eng. Sci.* 19 (2002) 357–372.
- [8] H. Winters, Twenty years experience in seawater reverse osmosis and how chemicals in pretreatment affect fouling of membranes, *Desalination* 110 (1997) 93–96.
- [9] K. Košutić, B. Kunst, Removal of organics from aqueous solutions by commercial RO and NF membranes of characterized porosities, *Desalination* 142 (2002) 47–56.
- [10] H. Ozaki, H. Li, Rejection of organics compounds by ultra-low pressure reverse osmosis membrane, *Water Res.* 36 (2002) 123–130.
- [11] L. Kaštelan-Kunst, K. Košutić, V. Dananić, B. Kunst, FT30 membranes of characterized porosities in the reverse osmosis organics removal from aqueous solutions, *Water Res.* 31 (1997) 2878–2884.
- [12] V. Tödtheide, G. Laufenberg, B. Kunz, Waste water treatment using reverse osmosis: real osmotic pressure and chemical functionality as influencing parameters on the retention of carboxylic acids in multi-component systems, *Desalination* 110 (1997) 213–222.
- [13] Y. Kiso, T. Kitao, K. Jinno, M. Miyagi, The effects of molecular weight on permeation of organic solute through cellulose acetate reverse osmosis membranes, *J. Membr. Sci.* 74 (1992) 95–103.
- [14] H.H.P. Fang, E.S.K. Chian, Reverse osmosis separation of polar organic compounds in aqueous solution, *Environ. Sci. Technol.* 10 (1976) 364–369.
- [15] W.A. Duvel Jr., T. Helfgott, Removal of wastewater organics by reverse osmosis, *J. Water Pollut. Control Fed.* 47 (1975) 57–65.
- [16] M.A. Ottinger, M. Abdelnabi, M. Quinn, N. Golden, J. Wu, N. Thompson, Reproductive consequences of EDCs in birds: What do laboratory effects mean in field species? *Neurotoxicol. Teratol.* 24 (2002) 17–28.
- [17] G.M. Solomon, T. Schettler, *Environment and health. 6. Endocrine disruption and potential human health implications*, *Can. Med. Assoc. J.* 163 (2000) 1471–1476.
- [18] J.E. Harries, D.A. Sheahan, S. Jobling, P. Matthiessen, M. Neall, J.P. Sumpter, T. Taylor, N. Zaman, Estrogenic activity in five United Kingdom rivers detected by measurement of vitellogenesis in caged male trout, *Environ. Toxicol. Chem.* 16 (1997) 534–542.
- [19] R.A. Hess, D. Bunick, K.H. Lee, J. Bahr, J.A. Taylor, K.S. Korach, D.B. Lubahn, A role for estrogens in the male reproductive system, *Nature* 390 (1997) 509–512.
- [20] C. Carey, C.J. Bryant, Possible interrelations among environmental toxicants, amphibian development, and decline of amphibian populations, *Environ. Health Persp.* 103 (1995) 13–17.
- [21] C.F. Face mire, T.S. Gross, L.J. Guillette, Reproductive impairment in the Florida panther: Nature or nurture? *Environ. Health Persp.* 103 (1995) 79–86.
- [22] C.E. Purdom, P.A. Hardiman, V.J. Bye, N.C. Eno, C.R. Tyler, J.P. Sumpter, Estrogenic effects of effluents from sewage treatment works, *J. Chem. Ecol.* 8 (1994) 275–285.
- [23] P. Lipp, R. Gimbel, F.H. Frimmel, Parameters influencing the rejection properties of FT30 membranes, *J. Membr. Sci.* 95 (1994) 185–197.
- [24] C.W. van Oers, M.A.G. Vorstman, P.J.A.M. Kerkhof, Solute rejection in the presence of a deposited layer during ultrafiltration, *J. Membr. Sci.* 107 (1995) 173–192.
- [25] J.M. Jackson, D. Landolt, About the mechanism of formation of iron hydroxide fouling layers on reverse osmosis membranes, *Desalination* 12 (1973) 361–378.
- [26] E. Staude, W. Assenmacher, A contribution to fouling in hyperfiltration induced by chemical reaction, *Desalination* 49 (1984) 215–228.
- [27] E.M. Vrijenhoek, S. Hong, M. Elimelech, Influence of membrane surface properties on initial rate of colloidal fouling of reverse osmosis and nanofiltration membranes, *J. Membr. Sci.* 188 (2001) 115–128.
- [28] A.L. Zydney, Stagnant film model for concentration polarization in membrane systems, *J. Membr. Sci.* 130 (1997) 275–281.
- [29] R.H. Davis, Modeling of fouling of cross-flow microfiltration membranes, *Sep. Purif. Meth.* 21 (1992) 75–126.
- [30] E.M.V. Hoek, M. Elimelech, Cake-enhanced concentration polarization: a new fouling mechanism for salt-rejecting membrane, *Environ. Sci. Technol.* 37 (2003) 5581–5588.
- [31] W.F. Blatt, A. Dravid, A.S. Michaels, L. Nelson, Solute polarization and cake formation in membrane ultrafiltration: causes, consequences, and control techniques, in: J.E. Flinn (Ed.), *Membrane Science and Technology: Industrial, Biological, and Waste Treatment Processes*, Plenum Press, New York, NY, pp. 47–97.
- [32] B.P. Boudreau, The diffusive tortuosity of fine-grained un lithified sediments, *Geochim. Cosmochim. Acta* 60 (1996) 3139–3142.
- [33] A. Seidel, M. Elimelech, Coupling between chemical and physical interactions in natural organic matter (NOM) fouling of nanofiltration membranes: implication for fouling control, *J. Membr. Sci.* 203 (2003) 245–255.
- [34] L.D. Nghiem, A.I. Schäfer, Adsorption and transport of trace contaminant estrone in NF/RO membranes, *Environ. Eng. Sci.* 19 (2002) 441–451.
- [35] L.D. Nghiem, A.I. Schäfer, T.D. Waite, Adsorption of estrone on nanofiltration and reverse osmosis membranes in water and wastewater treatment, *Water Sci. Technol.* 46 (2002) 265–272.
- [36] L.D. Nghiem, A.I. Schäfer, M. Elimelech, Removal of natural hormones by nanofiltration membranes: measurement, modeling, and mechanisms, *Environ. Sci. Technol.* 38 (2004) 1888–1896.